

# Summary of the Precision Measurements of the Electroweak Mixing Angle in the Region of the Z pole

Arie Bodek<sup>1</sup>, Hyon-San Seo<sup>1</sup>, and Un-Ki Yang<sup>2</sup>

<sup>1</sup>*Department of Physics and Astronomy, University of Rochester, Rochester, NY 14627, USA*

<sup>2</sup>*Department of Physics and Astronomy, Seoul National University, Seoul 151-747, Korea*

*Presented by Hyon-San Seo at the 32nd International Symposium on Lepton Photon Interactions at High Energies,  
Madison, Wisconsin, USA, August 25–29, 2025*

## Abstract

This contribution presents a overview of a recent CMS-based determination of the effective leptonic weak mixing angle,  $\sin^2 \theta_{\text{eff}}^\ell$ , derived from forward–backward asymmetry measurements in Drell–Yan events at 13 TeV [1]. Although the CMS analysis achieved a major reduction in uncertainties, its overall precision is ultimately limited by residual parton distribution function (PDF) uncertainties. This proceeding highlights the role of complementary CMS observables, which probe distinct parton-density combinations and provide additional constraints beyond those obtained from the original asymmetry measurement alone. The improved analysis yields a substantially reduced total uncertainty, resulting in  $\sin^2 \theta_{\text{eff}}^\ell = 0.23156 \pm 0.00024$ . This result is consistent with the Standard Model prediction and represents the highest precision achieved so far in an individual determination of this parameter.

## 1 Introduction

The effective leptonic weak mixing angle ( $\sin^2 \theta_{\text{eff}}^\ell$ ) is a key parameter in precision tests of the Standard Model (SM). A recent CMS analysis of the forward-backward asymmetry ( $A_{\text{FB}}$ ) in Drell–Yan events at 13 TeV [2] achieved a landmark precision, comparable to results from electron-positron LEP/SLD colliders. Despite the high experimental precision achieved by the CMS analysis, uncertainties related to the proton’s parton distribution functions (PDFs) remain the dominant limitation.

This work summarizes the results obtained using an extended PDF profiling strategy applied to the CMS measurement. We incorporate additional, powerful constraints from CMS measurements of the  $W$ -boson decay lepton asymmetry [3] and  $W/Z$  cross-section ratios [4]. After establishing consistency with the published CMS measurement, the extended fit strategy leads to a noticeable reduction in the PDF-driven component of the total uncertainty. This approach results in the most precise single measurement of  $\sin^2 \theta_{\text{eff}}^\ell$  to date.

## 2 Reproduction of the CMS 13 TeV analysis

The CMS extraction of the weak mixing angle is based on a global fit framework that incorporates correlated experimental and theoretical uncertainties [2].

$$\chi^2(\beta_{\text{exp}}, \beta_{\text{th}}) = \sum_i \frac{(\sigma_i^{\text{exp}} + \sum_j \Gamma_{ij}^{\text{exp}} \beta_{j,\text{exp}} - \sigma_i^{\text{th}} - \sum_k \Gamma_{ik}^{\text{th}} \beta_{k,\text{th}})^2}{\Delta_i^2} + \sum_j \beta_{j,\text{exp}}^2 + \sum_k \beta_{k,\text{th}}^2. \quad (1)$$

Correlated experimental and theoretical uncertainties are implemented by introducing nuisance parameters,  $\beta_{\text{exp}}$  and  $\beta_{\text{th}}$ , which propagate their effects to the measured spectra and theoretical predictions through

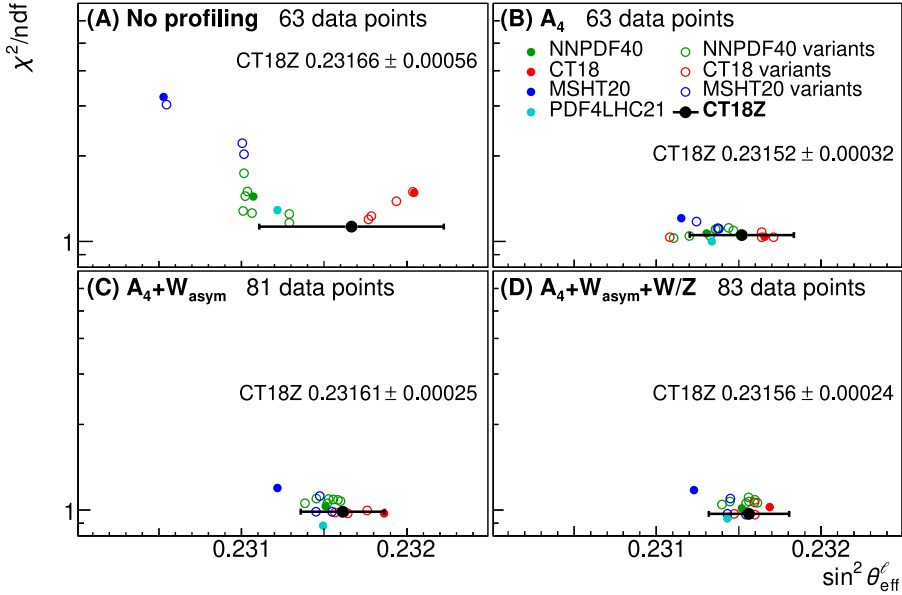


Figure 1: Extracted values of  $\sin^2 \theta_{\text{eff}}^{\ell}$  from the 13 TeV CMS  $A_4$  data for 19 different PDF sets on the horizontal axis. (A) Before profiling. (B) After profiling with  $A_4$ . (C) After profiling with  $A_4$  plus  $W$  decay lepton asymmetry. (D) After profiling with  $A_4$  plus  $W$  decay lepton asymmetry plus  $W/Z$  cross section ratios. The vertical axis shows the  $\chi^2$  values of the fits divided by the number of degrees of freedom ( $N_{\text{data}} - 1$ ), where the one degree of freedom corresponds to the free parameter  $\sin^2 \theta_{\text{eff}}^{\ell}$ .

the corresponding response matrices  $\Gamma^{\text{exp}}$  and  $\Gamma^{\text{th}}$ . Within this framework, the index  $i$  labels the  $N_{\text{data}}$  points of the  $(|y|, M)$  double-differential  $A_4$  dataset, corresponding to 63 entries used in the  $A_4$  profiling. The indices  $j$  and  $k$  index the nuisance parameters associated with experimental and theoretical uncertainty sources, respectively. The measured values and their uncorrelated experimental uncertainties are denoted by  $\sigma_i^{\text{exp}}$  and  $\Delta_i$ , while the theoretical predictions are given by  $\sigma_i^{\text{th}}$ . Correlations among experimental uncertainties in the double-differential  $A_4$  measurement are accounted for by the covariance matrix  $\Gamma^{\text{exp}}$ .

Modern QCD calculations are used to model the Drell–Yan process, following the setup of the original CMS analysis [5–9]. And the  $Z$ -boson transverse-momentum spectrum is reweighted to data, following the original CMS analysis.

The theoretical uncertainty accounts for effects arising from missing higher-order contributions in both QCD and electroweak (EW) calculations. Electroweak corrections are evaluated using POWHEG-Z\_EW, while PDF-related uncertainties are derived from NLO grids produced with MADGRAPH5-AMC@NLO [10] and interfaced through PINEAPPL [11, 12]. These components are incorporated into the matrix  $\Gamma^{\text{th}}$  via nuisance parameters that represent missing higher-order EW effects, PDF Hessian variations, and the effective weak mixing angle  $\sin^2 \theta_{\text{eff}}^{\ell}$  itself, which is treated as a free parameter in the fit. Uncertainties associated with missing higher-order QCD corrections are assessed by repeating the fit under six independent scale variations, with the largest observed deviation from the nominal result taken as the corresponding uncertainty.

Table 1 summarizes the extracted values of  $\sin^2 \theta_{\text{eff}}^{\ell}$ , expressed in units of  $10^{-5}$ , obtained with the 13 TeV  $A_4$  distribution both prior to and following the profiling procedure, for a total of 19 PDF sets. The majority of these PDFs are computed at next-to-next-to-leading-order (NNLO) accuracy in QCD, while a subset corresponds to approximate next-to-next-to-next-to-leading-order calculations (an3lo). PDF ensembles marked as “qed” incorporate Quantum Electrodynamics effects and explicitly include photon parton densities. Within the NNPDF40 family, the “mhou” designation denotes the inclusion of corrections associated with missing higher-order uncertainties. The MSHT and NNPDF sets adopt asymmetric parameterizations of the strange-quark sea, whereas the CTEQ sets assume a symmetric strange-quark sea, with the exception of the CT18As PDF.

The total uncertainties in Table 1 include contributions from statistical, experimental systematic, theo-

PDF	A <sub>4</sub> without profiling (63 data points)			A <sub>4</sub> profiling (63 data points)			A <sub>4</sub> + W <sub>asym</sub> + W/Z profiling (83 data points)		
	sin <sup>2</sup> θ <sub>eff</sub> <sup>ℓ</sup>	Diff. from CT18Z	χ <sup>2</sup>	sin <sup>2</sup> θ <sub>eff</sub> <sup>ℓ</sup>	Diff. from CT18Z	χ <sup>2</sup>	sin <sup>2</sup> θ <sub>eff</sub> <sup>ℓ</sup>	Diff. from CT18Z	χ <sup>2</sup>
NNPDF40									
nnlo_as_01180_hessian [15]	23107 ± 49	-59	89	23130 ± 24	-22	66	23152 ± 23	-4	83
nnlo_as_01180_qed [16]	23102 ± 46	-64	108	23144 ± 23	-8	69	23161 ± 22	5	87
nnlo_as_01180_mhou [17]	23101 ± 45	-65	79	23110 ± 27	-42	64	23145 ± 24	-11	88
nnlo_as_01180_qed_mhou [16]	23103 ± 46	-63	93	23136 ± 24	-16	69	23156 ± 23	0	88
an3lo_as_01180 [18]	23129 ± 46	-37	72	23132 ± 25	-20	65	23154 ± 23	-2	87
an3lo_as_01180_qed [18]	23129 ± 49	-37	78	23147 ± 23	-5	68	23160 ± 22	4	89
an3lo_as_01180_mhou [18]	23106 ± 47	-60	78	23120 ± 26	-32	65	23140 ± 25	-16	86
an3lo_as_01180_qed_mhou [18]	23102 ± 44	-64	90	23137 ± 23	-15	69	23156 ± 23	0	91
CTEQ									
CT18NNLO [19]	23204 ± 64	38	92	23166 ± 36	14	64	23169 ± 24	13	84
<b>CT18Znnlo</b> [19]	23166 ± 56	0	70	23152 ± 32	0	65	<b>23156 ± 24</b>	0	79
CT18ANNLO [19]	23179 ± 54	13	76	23164 ± 28	12	67	23160 ± 23	4	79
CT18XNNLO [19]	23194 ± 53	28	86	23171 ± 30	19	64	23160 ± 24	4	87
CT18QED-PROTON [20]	23204 ± 64	38	93	23164 ± 36	12	64	23155 ± 24	-1	80
CT18As_LATNNLO [21]	23177 ± 75	11	74	23108 ± 43	-44	64	23147 ± 35	-9	80
MSHT20									
MSHT20nnlo_as118 [22]	23053 ± 46	-113	200	23115 ± 30	-37	75	23123 ± 26	-33	96
MSHT20qed_nnlo [23]	23055 ± 59	-111	188	23124 ± 31	-28	73	23145 ± 27	-11	90
MSHT20an3lo_as118 [24]	23101 ± 47	-65	138	23138 ± 29	-14	69	23154 ± 26	-2	79
MSHT20qed_an3lo [25]	23101 ± 52	-65	126	23137 ± 31	-15	69	23143 ± 28	-13	80
PDF4LHC21_40 [26]	23122 ± 83	-44	80	23133 ± 33	-19	62	23143 ± 27	-13	77

Table 1: Values of  $\sin^2 \theta_{\text{eff}}^{\ell}$  (in units of  $10^{-5}$ ) before and after profiling with the CMS 13 TeV  $A_4$  distribution (63 points) for 19 PDF sets. Also shown are the values extracted by including the CMS 13 TeV  $W$ -decay lepton asymmetry and the CMS  $W/Z$  cross section ratios (total of 83 points) in the profiling. The total uncertainties include contributions from statistical, experimental systematic, theoretical and PDF sources. The column marked "Diff. from CT18Z" is the difference from  $\sin^2 \theta_{\text{eff}}^{\ell}$  extracted with the CT18ZNNLO PDF set. Note, the  $\chi^2$  values before profiling do not include PDF errors, while the  $\chi^2$  values after profiling include PDF errors.

retical, and PDF sources. The differences in the results obtained with the various PDF sets (*before profiling*) largely reflect variations in input datasets, parameterization choices, and flavor assumptions. If there are sufficient parameters in the PDF sets, then the profiled PDFs should be able to describe all data that are used in the  $\sin^2 \theta_{\text{eff}}^{\ell}$  profiling analysis with good  $\chi^2$ . The columns labeled marked "Diff. from CT18Z" show the difference between the value of  $\sin^2 \theta_{\text{eff}}^{\ell}$  extracted with each of the 19 PDF sets and that obtained using the nominal CT18ZNNLO PDF set.

For the nominal CT18ZNNLO set, the profiled value obtained from the 13 TeV  $A_4$  data alone is in very good agreement with the published CMS result (Table 1), which validates our implementation of the CMS analysis in xFITTER [13, 14].

### 3 Extended Profiling with $W$ Charge Asymmetry and $W/Z$ Cross Section Ratios

After profiling, the dominant PDF uncertainty is largely reduced, but small differences between modern PDF sets are still observed. As shown in [27], including the  $W$ -boson charge asymmetry measurements ( $W_{\text{asym}}$ ) in the profiling provides additional constraints on the  $d/u$  ratio, leading to a further reduction of the PDF uncertainty in  $\sin^2 \theta_{\text{eff}}^{\ell}$ . Moreover, some CT18 PDF sets lack sufficient constraints on the strange-quark distribution at high energy scales, resulting in systematically lower strange-quark densities compared to other PDFs and thereby predicting a larger effective weak mixing angle. Incorporating the  $W/Z$  cross section ratios can provide further constraints on the strange-quark distribution, helping to reduce these discrepancies.

Therefore, we perform an updated analysis of the published CMS 13 TeV  $A_4$  data (63 data points). We also include the recent CMS  $W_{\text{asym}}$  measurement [3] at 13 TeV (18 additional data points) and the CMS measurements of the  $W$  and  $Z$  fiducial cross-section ratios [4] at 5.02 TeV ( $12.505 \pm 0.037_{\text{stat}} \pm 0.032_{\text{syst}}$ ) and 13 TeV ( $12.078 \pm 0.028_{\text{stat}} \pm 0.032_{\text{syst}}$ ), contributing 2 additional data points. The results are shown in the columns of Table 1 and in Figure 1.

Extracted values of  $\sin^2 \theta_{\text{eff}}^\ell$  from the 13 TeV CMS  $A_4$  data for different PDF sets are shown on the horizontal axis of each of the four panels in Fig. 1. The vertical axis shows the values of  $\chi^2$  normalized to the number of degrees of freedom,  $\text{ndf} = N_{\text{data}} - 1$ , where the subtraction accounts for the single free parameter  $\sin^2 \theta_{\text{eff}}^\ell$ . Shown are the values before profiling (panel A, 63 data points). After profiling with  $A_4$  (panel B, 63 data points), after profiling with  $A_4$  and also with  $W$  decay lepton asymmetry (panel C, 81 data points), and after profiling with  $A_4$  and the  $W$  decay lepton asymmetry and also the  $W/Z$  cross section ratios (panel D, 83 data points).

As seen in Table 1 and Figure 1, after  $A_4$  profiling the error in the extracted value of  $\sin^2 \theta_{\text{eff}}^\ell$  with the nominal CT18ZNNLO PDF set is reduced from 0.00056 to 0.00032. By also including the  $W$  decay lepton asymmetry and the  $W/Z$  cross section ratios the uncertainty for the nominal CT18ZNNLO is reduced to 0.00024.

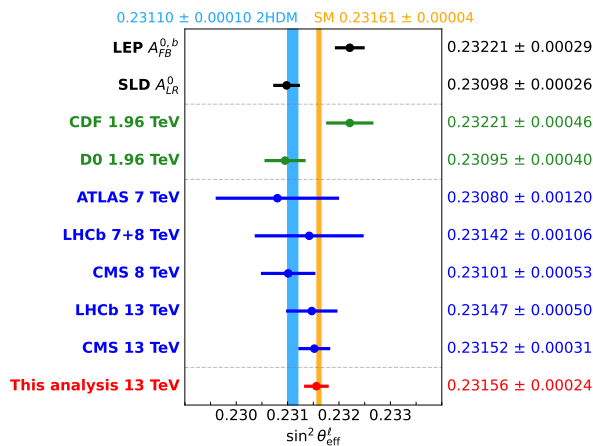


Figure 2: Comparison of  $\sin^2 \theta_{\text{eff}}^\ell$  extracted in this analysis (labeled "This analysis 13 TeV") with previous measurements [2, 28–34] and the prediction of the 2025 SM global fit [35, 36]. Also shown is the prediction of the Two Higgs Doublet Model [37] corresponding to the CDF  $M_W$  value [38] ( $80.4335 \pm 0.0094$  GeV).

Including all three inputs in the profiling procedure results in a pronounced alignment among the different PDF sets. Following profiling, the extracted central values from 18 of the 19 PDFs (including three of the four MSHT20 sets) are consistent with the CT18ZNNLO determination at the level of one standard deviation. The only exception is the profiled MSHT20NNLO\_AS118 set, whose central value lies 1.38 standard deviations below the CT18ZNNLO result and is associated with a poor  $\chi^2$ . By contrast, as reported in Table 1, the profiled MSHT20AN3LO\_AS118 set yields an identical value of  $\sin^2 \theta_{\text{eff}}^\ell$  to that obtained with CT18ZNNLO, together with an acceptable  $\chi^2$ .

Figure 2 shows a comparison of  $\sin^2 \theta_{\text{eff}}^\ell$  extracted in this analysis with the nominal CT18ZNNLO PDF set (Labeled "This analysis 13 TeV") to previous measurements [2, 28–34]. Also shown are the predictions of the 2025 SM global fit [35, 36] and the prediction of the Two Higgs Doublet Model [37] assuming the CDF  $M_W$  value [38] of  $80.4335 \pm 0.0094$  GeV.

## 4 Conclusion

This proceeding reports on a CMS-based analysis in which additional  $W$ -boson charge asymmetry and  $W/Z$  cross-section measurements are used to further constrain parton distribution effects in the determination of  $\sin^2 \theta_{\text{eff}}^\ell$ . The final result,  $\sin^2 \theta_{\text{eff}}^\ell = 0.23156 \pm 0.00024$ , represents the most precise single measurement of this parameter to date, obtained by combining collider measurements with PDF-sensitive observables, as presented in Ref. [1]. A key output of this enhanced profiling is the excellent consistency observed across different 18 PDFs, yielding results within one standard deviation of the nominal CT18ZNNLO value. The extracted value is compatible with the Standard Model expectation,  $\sin^2 \theta_{\text{eff}}^\ell = 0.23161 \pm 0.00004$ .

Research supported by the U.S. Department of Energy under University of Rochester grant number DE-SC0008475 and by National Research Foundation of Korea (NRF) grants (RS-2024-00350406, RS-2008-NR007227).

## References

- [1] Arie Bodek, Hyon-San Seo, and Un-Ki Yang. Precision Measurements of the Electroweak Mixing Angle in the Region of the  $Z$  pole. 8 2025. arXiv:2508.18022 (to be published in Physics Reports).
- [2] Aram Hayrapetyan et al. Measurement of the Drell-Yan forward-backward asymmetry and of the effective leptonic weak mixing angle in proton-proton collisions at  $\sqrt{s} = 13$  TeV. *Phys. Lett. B*, 866:139526, 2025.
- [3] Albert M Sirunyan et al. Measurements of the  $W$  boson rapidity, helicity, double-differential cross sections, and charge asymmetry in  $pp$  collisions at  $\sqrt{s} = 13$  TeV. *Phys. Rev. D*, 102(9):092012, 2020.

[4] Aram Hayrapetyan et al. Measurement of the inclusive cross sections for  $W$  and  $Z$  boson production in proton-proton collisions at  $\sqrt{s} = 5.02$  and  $13$  TeV. *JHEP*, 04:162, 2025.

[5] Pier Francesco Monni, Emanuele Re, and Marius Wiesemann. MiNNLO<sub>PS</sub>: optimizing  $2 \rightarrow 1$  hadronic processes. *Eur. Phys. J. C*, 80(11):1075, 2020.

[6] Piotr Gonokna and Zbigniew Was. PHOTOS Monte Carlo: A Precision tool for QED corrections in  $Z$  and  $W$  decays. *Eur. Phys. J. C*, 45:97–107, 2006.

[7] Mauro Chiesa, Fulvio Piccinini, and Alessandro Vicini. Direct determination of  $\sin^2 \theta_{\text{eff}}^\ell$  at hadron colliders. *Phys. Rev. D*, 100(7):071302, 2019.

[8] Mauro Chiesa, Clara Lavinia Del Pio, and Fulvio Piccinini. On electroweak corrections to neutral current Drell-Yan with the POWHEG BOX. *Eur. Phys. J. C*, 84:539, 2024.

[9] Luca Barze, Guido Montagna, Paolo Nason, Oreste Nicolsini, Fulvio Piccinini, and Alessandro Vicini. Neutral current Drell-Yan with combined QCD and electroweak corrections in the POWHEG BOX. *Eur. Phys. J. C*, 73(6):2474, 2013.

[10] J. Alwall, R. Frederix, S. Frixione, V. Hirschi, F. Maltoni, O. Mattelaer, H. Shao, T. Stelzer, P. Torrielli, and M. Zaro. The automated computation of tree-level and next-to-leading order differential cross sections, and their matching to parton shower simulations. *JHEP*, 07:079, 2014.

[11] Christopher Schwan. PineAPPL: NLO EW corrections for PDF processes. *SciPost Phys. Proc.*, 8:079, 2022.

[12] S. Carrazza, E. R. Nocera, C. Schwan, and M. Zaro. PineAPPL: combining EW and QCD corrections for fast evaluation of LHC processes. *JHEP*, 12:108, 2020.

[13] S. Alekhin et al. HERAFitter. *Eur. Phys. J. C*, 75:304, 2015.

[14] S. Camarda et al. QCD analysis of  $W$ - and  $Z$ -boson production at Tevatron. *Eur. Phys. J. C*, 75:458, 2015.

[15] Richard D. Ball et al. The path to proton structure at 1% accuracy. *Eur. Phys. J. C*, 82(5):428, 2022.

[16] Richard D. Ball et al. Photons in the proton: implications for the LHC. *Eur. Phys. J. C*, 84(5):540, 2024.

[17] Richard D. Ball et al. Determination of the theory uncertainties from missing higher orders on NNLO parton distributions with percent accuracy. *Eur. Phys. J. C*, 84:517, 2024.

[18] Richard D. Ball et al. The path to  $N^3\text{LO}$  parton distributions. *Eur. Phys. J. C*, 84(7):659, 2024.

[19] Tie-Jiun Hou et al. New CTEQ global analysis of quantum chromodynamics with high-precision data from the LHC. *Phys. Rev. D*, 103(1):014013, 2021.

[20] Keping Xie, Bei Zhou, and T. J. Hobbs. The photon content of the neutron. *JHEP*, 04:022, 2024.

[21] Tie-Jiun Hou, Huey-Wen Lin, Mengshi Yan, and C. P. Yuan. Impact of lattice strangeness asymmetry data in the CTEQ-TEA global analysis. *Phys. Rev. D*, 107:076018, 2023.

[22] S. Bailey, T. Cridge, L. A. Harland-Lang, A. D. Martin, and R. S. Thorne. Parton distributions from LHC, HERA, Tevatron and fixed target data: MSHT20 PDFs. *Eur. Phys. J. C*, 81(4):341, 2021.

[23] T. Cridge, L. A. Harland-Lang, A. D. Martin, and R. S. Thorne. QED parton distribution functions in the MSHT20 fit. *Eur. Phys. J. C*, 82(1):90, 2022.

[24] J. McGowan, T. Cridge, L. A. Harland-Lang, and R. S. Thorne. Approximate  $N^3\text{LO}$  parton distribution functions with theoretical uncertainties: MSHT20aN $^3\text{LO}$  PDFs. *Eur. Phys. J. C*, 83(3):185, 2023. [Erratum: Eur.Phys.J.C 83, 302 (2023)].

[25] Thomas Cridge, Lucian A. Harland-Lang, and Robert S. Thorne. Combining QED and approximate  $N^3\text{LO}$  QCD corrections in a global PDF fit: MSHT20qed\_an3lo PDFs. *SciPost Phys.*, 17(1):026, 2024.

[26] Richard D. Ball et al. The PDF4LHC21 combination of global PDF fits for the LHC Run III. *J. Phys. G*, 49:080501, 2022.

[27] A. Bodek, J. Han, A. Khukhunaishvili, and W. Sakumoto. Using Drell-Yan forward-backward asymmetry to reduce PDF uncertainties in the measurement of electroweak parameters. *Eur. Phys. J. C*, 76(3):115, 2016.

[28] S. Schael et al. Precision electroweak measurements on the  $Z$  resonance. *Phys. Rept.*, 427:257–454, 2006.

[29] Timo Antero Aaltonen et al. Measurement of  $\sin^2 \theta_{\text{eff}}^{\text{lept}}$  using  $e^+e^-$  pairs from  $\gamma^*/Z$  bosons produced in  $p\bar{p}$  collisions at a center-of-momentum energy of  $1.96$  TeV. *Phys. Rev. D*, 93(11):112016, 2016. [Addendum: Phys.Rev.D 95, 119901 (2017)].

[30] Victor Mukhamedovich Abazov et al. Measurement of the Effective Weak Mixing Angle in  $p\bar{p} \rightarrow Z/\gamma^* \rightarrow \ell^+\ell^-$  Events. *Phys. Rev. Lett.*, 120(24):241802, 2018.

[31] Georges Aad et al. Measurement of the forward-backward asymmetry of electron and muon pair-production in  $pp$  collisions at  $\sqrt{s} = 7$  TeV with the ATLAS detector. *JHEP*, 09:049, 2015.

[32] Albert M. Sirunyan et al. Measurement of the weak mixing angle using the forward-backward asymmetry of Drell-Yan events in  $pp$  collisions at  $\sqrt{s} = 8$  TeV. *Eur. Phys. J. C*, 78(9):701, 2018.

[33] Roel Aaij et al. Measurement of the forward-backward asymmetry in  $Z/\gamma^* \rightarrow \mu^+\mu^-$  decays and determination of the effective weak mixing angle. *JHEP*, 11:190, 2015.

[34] R. Aaij et al. Measurement of the effective leptonic weak mixing angle. *JHEP*, 12:026, 2024.

[35] S. Navas et al. Review of particle physics. *Phys. Rev. D*, 110(3):030001, 2024.

[36] S. Navas et al. Review of particle physics 2025 online update, 2025.

[37] Thomas Biekötter, Sven Heinemeyer, and Georg Weiglein. Excesses in the low-mass Higgs-boson search and the  $W$ -boson mass measurement. *Eur. Phys. J. C*, 83(5):450, 2023.

[38] T. Aaltonen et al. High-precision measurement of the  $W$  boson mass with the CDF II detector. *Science*, 376(6589):170–176, 2022.